33RD CONGRESS
OF THE INTERNATIONAL COUNCIL
OF THE AERONAUTICAL SCIENCES
STOCKHOLM, SWEDEN, 4-9 SEPTEMBER, 2022

ICAS 2022 SWEDEN

Variations in Structural Properties of Lattice Structures Depending on Unit Cell Shape for Morphing Wings

Yuta Nishijima[1], Hiroaki Tanaka[1], Adrian Biron[2] & Takashi Miura[1]

[1]Department of Aerospace Engineering, National Defense Academy, Yokosuka, Kanagawa 239-8686, Japan
[2]Department of Mechanical Engineering, Special Military School of Saint-Cyr, Guer 56380, France

Abstract

Lattice structures are created via a regular arrangement of unit cells and the structural characteristics of the entire lattice structure can be changed significantly by altering the structure of the unit cells. This property allows morphing wings to exhibit anisotropic structural characteristics that can be varied in some sections; additionally, it allows them to be lightweight in arbitrary proportions while maintaining the necessary stiffness. In this study, five types of lattice structures are employed and their structural characteristics are investigated. They are subjected to bending, tensile, compressive, and torsional tests, and the equivalent stiffness of each lattice is calculated. Differences in their structural characteristics can be used to achieve various types of wing morphing for different applications. In this study, wing twist morphing is developed using the cube lattice, which exhibits high equivalent bending stiffness and low equivalent torsional stiffness. Subsequently, a wing prototype is developed to evaluate the structural properties of the morphing wing. Bending and torsion tests are conducted on the wing, and the equivalent bending and torsional stiffness are calculated. Results show that the equivalent torsional stiffness increased, as compared with that of the cube lattice specimen. This is attributable to the wing chord length being larger than the width of the specimen, which increases the equivalent torsional stiffness. Although the thickness of the wing changed only slightly, the change in the equivalent bending stiffness is suppressed.

Keywords: morphing wing, lattice structure, 3D printing

1. Introduction

Lattice structures have garnered considerable attention in recent years. A lattice structure is a three-dimensional (3D) patterned structure that can exhibit physical properties different from those of a single material depending on the unit cell shape [1]. Previously, complex internal structures were difficult to manufacture; however, this issue has been alleviated via the use of 3D printers. The use of lattice structures [1] allows weight reduction [2], a change in the material density at any point, and the achievement of specific structural properties, such as stiffness anisotropy.

The ultimate goal of our study is to apply lattice structures to morphing wing systems [3,4]. A morphing wing is a wing whose shape can be changed smoothly based on its purpose [5,6]. For example, aircraft flaps and ailerons can be replaced by morphing wing systems. Typically, flaps and ailerons have hinges, which result in drag. Morphing wings eliminate the use of these hinges and change the wing shape seamlessly, thereby reducing the aerodynamic drag and potentially expanding the flight range. In addition, the morphing wing is expected to both optimize the lift–drag ratio by changing the wing shape based on the flight speed and significantly improve the short-range takeoff and landing performance via the large deformation of the wing. In this study, the basic structural characteristics of lattice structures are investigated and the applicability of lattice structures to morphing wing systems is discussed.

2. Structural Characterization of Basic Lattice Structures

2.1 Specimen for Structural Property Evaluation

Lattice structures consist of repeating unit cells in three dimensions; however, their structural properties vary significantly depending on the shape of the unit cell. We designed lattice structures with five different unit cell shapes based on space-filling polyhedral and crystal structures. The designed lattice structures are shown in Fig. 1.

The unit cell of the X-lattice comprises beams that connect the vertices of a cube. The unit cell of the cube (CUBE) lattice comprises beams that connect the edges of the cube. The unit cell of the octahedron (OCT) lattice is a space-filled octahedral structure with many triangles and is expected to exhibit high stiffness. The unit cell of the diamond lattice (DIA) is based on the crystal structure of diamonds and is expected to exhibit high stiffness. The unit cell of the rhombic dodecahedron (DODE) lattice is a space-filled rhombic dodecahedron and is expected to exhibit homogeneous stiffness in all directions.

The dimensions of the test model shown in the bottom row of Fig. 1 were set to obtain specimens that exhibit consistent widths and thicknesses to accommodate the experimental equipment. The length of the model was set to approximately 60 mm because the distance between the supporting pins of the bending test machine was 60 mm. The dimensions of the lattice structures are listed in Table 1. The test models were constructed using a Markforged Mark2 3D printer. The printer's stacking pitch ranged from 0.1 to 0.2 mm, and the test models were fabricated with a pitch of 0.1 mm. Markforged Onyx, which is a microcarbon-fiber-filled nylon, was used to fabricate the test models.

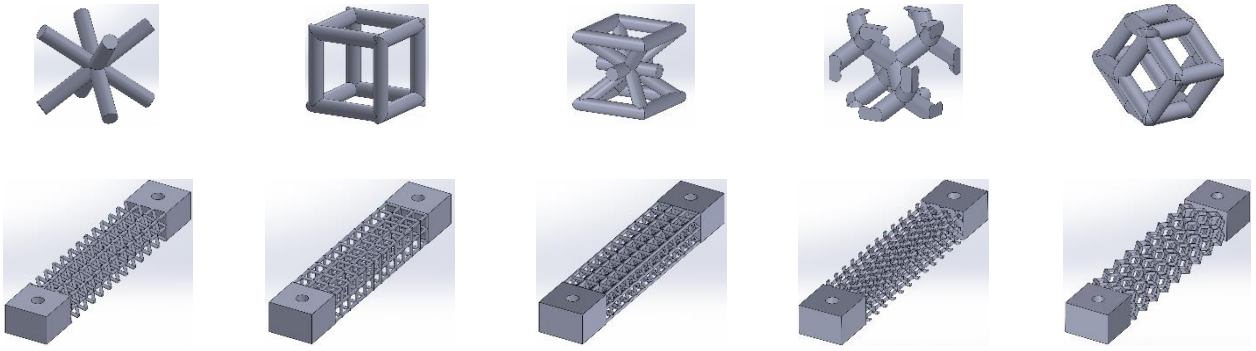

(a) X lattice (b) CUBE lattice (c) OCT lattice (d) DIA lattice (e) DODE lattice

Figure 1 - Lattice structures created in this study (top: unit cell structure; bottom: specimen)

Table 1 Dimensions of each test model (mm)

Dimensions	X lattice	CUBE lattice	OCT lattice	DIA lattice	DODE lattice
Beam diameter	1.0	1.0	1.0	1.0	1.0
Specimen width	15.0	16.0	16.0	15.0	16.0
Specimen thickness	10.0	11.0	11.0	10.0	11.0
Length of lattice	60.0	60.0	60.0	60.0	63.0

2.2 Experiments to Investigate Structural Properties of Lattice Structures

Four-point bending, tensile, and torsion tests were conducted to investigate the properties of the lattice structures.

2.2.1 Four-point bending

Figure 2 presents an overview of the four-point bending test. A testing machine (JT Tohsi, Little Senstar) was used for the four-point bending test. Load was measured using a load cell (Little Senstar) and displacement was measured using a laser displacement sensor (Keyence IL-100) from the underside of the specimen. The support span was 60 mm, distance between the load points was 20 mm, and displacement was applied.

Using the experimental results, the equivalent bending stiffness EI_{eq} can be obtained as follows.

$$EI_{eq} = \frac{23PL^3}{648\delta_b}, \qquad [N \cdot m^2] \tag{1}$$

where P denotes the load, L denotes the support span, and δ_b denotes the deformation.

Because the masses among the test models were different, we could not determine whether the change in stiffness was due to the structure or material density by comparing only the stiffness. Therefore, we divided the equivalent bending stiffness EI_{eq} by the density of the lattice section ρ to obtain the bending stiffness per density S_b, as follows.

$$S_b = \frac{EI_{eq}}{\rho}. \qquad \left[\frac{N \cdot m^5}{kg}\right] \tag{2}$$

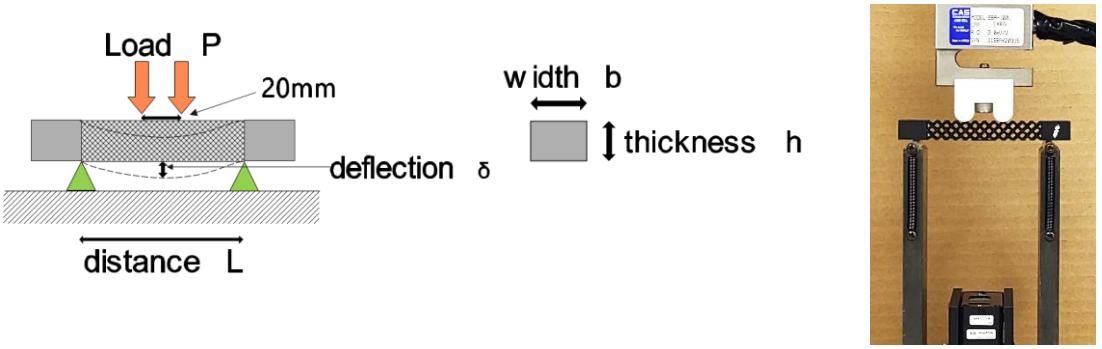

Figure 2 - Overview of four-point bending test
(left: schematic representation; right: photograph of test setup)

2.2.2 Tensile test

An overview of the tensile tests is presented in Fig. 3. The testing machine and load sensor were the same as those used for the four-point bending test, and displacement was measured from the crosshead movement of the testing machine. Both ends of the specimen were fixed with vises and tensile displacement was applied to the specimen.

Figure 3 - Overview of tensile test
(left: schematic representation; right: photograph of test setup)

2.2.3 Compression test

An overview of the compression test is shown in Fig. 4. The testing machine and sensor were identical to those used for the tensile test. A jig was attached to the lower end of the test model and a compressive displacement was applied to the specimen.

The equivalent tensile and compressive stiffnesses EA_{eq} are obtained as follows.

$$EA_{eq} = \frac{PL}{\delta_e}. \qquad [N] \tag{3}$$

Therefore, the tensile and compressive stiffnesses per density, S_e and S_c, respectively, are calculated as follows.

$$S_e = S_c = \frac{EA_{eq}}{\rho}. \qquad \left[\frac{N \cdot m^3}{kg}\right] \tag{4}$$

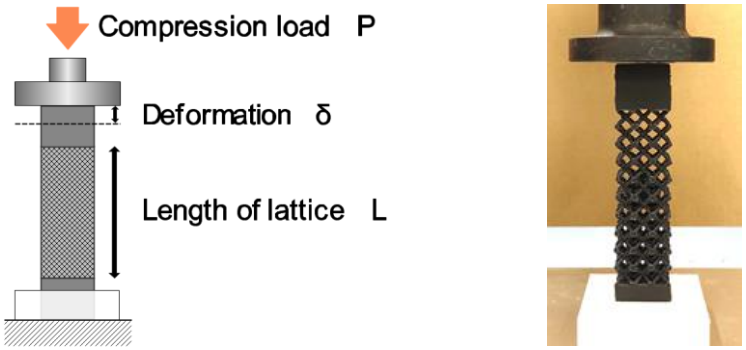

Figure 4 - Overview of compression test
(left: schematic representation; right: photograph of test setup)

2.2.4 Torsion test

An overview of the torsion test is shown in Fig. 5. We did not use a dedicated testing machine for the torsion test; therefore, we fabricated an experimental apparatus using a 3D printer. A 50 mm metal shaft was passed through the specimen and equal tensile loads were applied to the specimen from both sides using the Little Senstar testing machine. The twist angle was calculated from the shaft displacement measured using IL-100 and load was measured using a load cell (TKA-20A, Tokyo Sokki Co.). In this test, the torsional load was applied by tensile forces in the flexible cables, as indicated by the yellow lines in Fig. 5. As such, no axial load was applied to the specimen.

The equivalent torsional stiffness GJ_{eq} is calculated using the experimental results as follows.

$$GJ_{eq} = \frac{M_t}{\varphi} \times L, \qquad [N \cdot m^2] \tag{5}$$

where φ is the specific twist angle, and Mt is the applied torsional moment.

Therefore, the torsional stiffness per density, S_t, is calculated as follows.

$$S_t = \frac{GJ_{eq}}{\rho}. \qquad \left[N \cdot \frac{m^5}{kg}\right] \tag{6}$$

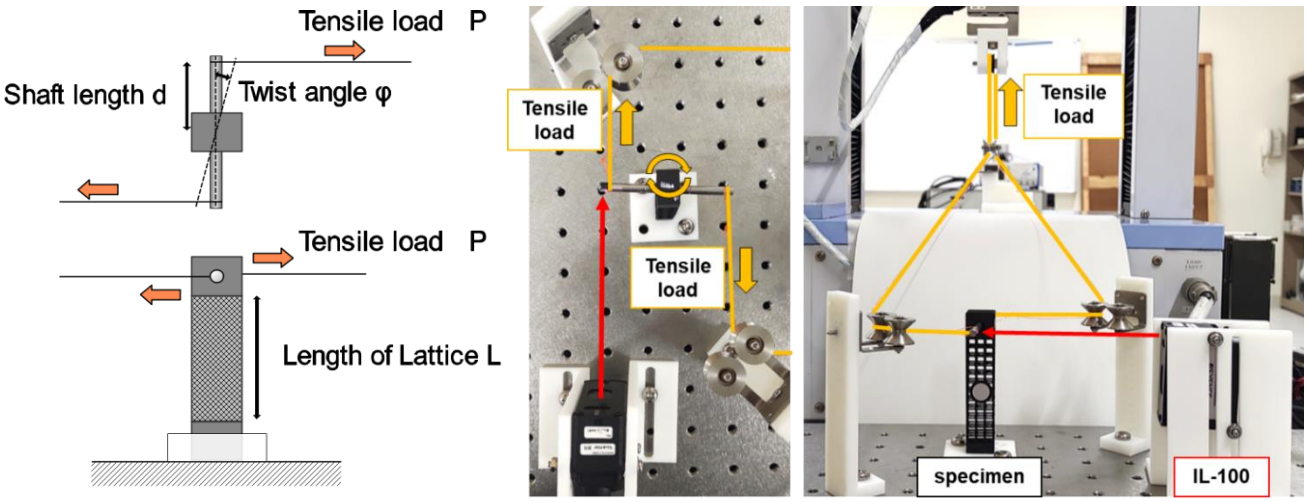

Figure 5 – Overview of torsion test
(left: schematic representation; right: photograph of test setup)

2.3 Experimental Results

The experimental results are presented in Figs. 6–9. The equivalent bending, tensile, compression, and torsional stiffnesses of each lattice structure were obtained from the experimental results. The characteristics of the lattice structures are listed in Table 2. The experimental results show that the stiffness values differed depending on the basic structure. The characteristics of these lattices are as follows. The X lattice is stiff in torsion but bends easily; the CUBE lattice is stiff in bending and tension but has a low torsional stiffness. In the compression test, the compressive load remained at approximately 50 N due to buckling in the structure. The OCT lattice is stiff in bending, tension, compression, and torsion; the DIA lattice is relatively stiff in tension, compression, and torsion but bends easily; and the DODE lattice exhibits low stiffness in bending, tension, compression, and torsion. This implies that the stiffness can be increased or decreased depending on the unit cell structures used. These differences in the structural characteristics can be exploited to achieve various types of wing morphings for different applications.

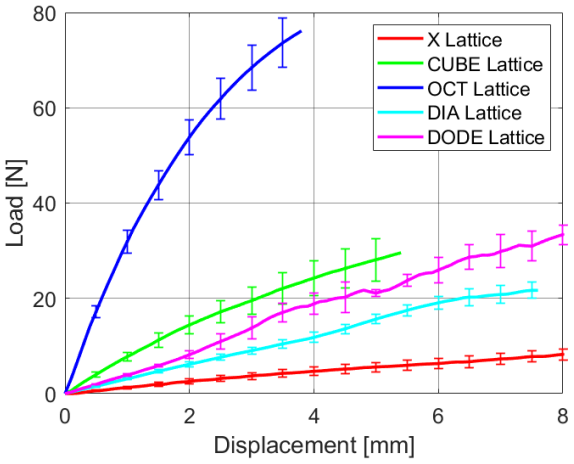

Figure 6 - Four-point bending test

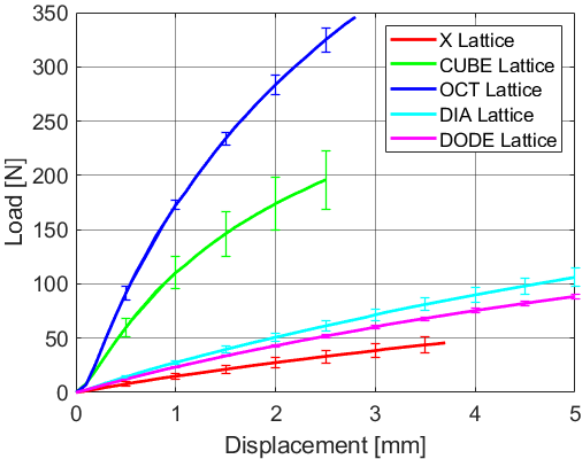

Figure 7 - Tensile test

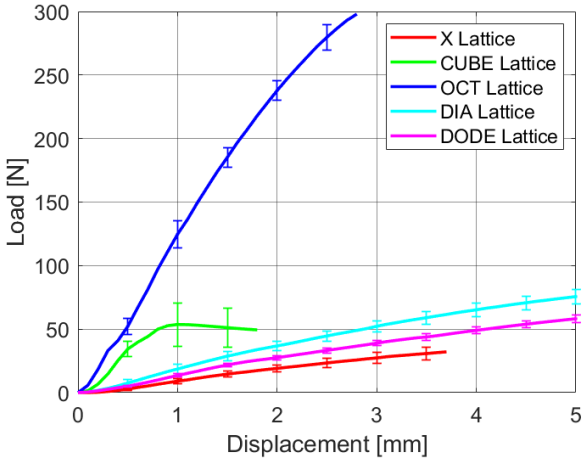

Figure 8 - Compression test

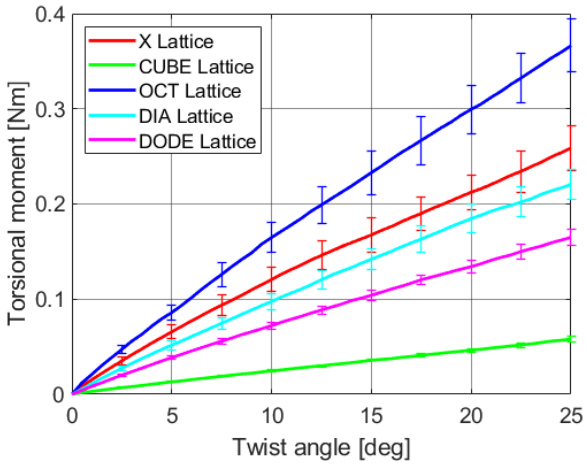

Figure 9 - Torsion test

Table 2 Dependence of structural properties on unit cell structure

Parameter	X lattice	CUBE lattice	OCT lattice	DIA lattice	DODE lattice
Mass of lattice part (g)	1.93	1.44	3.30	1.93	2.47
Density (kg/m^3)	214	136	313	214	223
Bending stiffness (N·m^2)	1.06×10^{-2}	5.79×10^{-2}	22.98×10^{-2}	2.39×10^{-2}	2.99×10^{-2}
Bending stiffness per density (N·m^5/kg)	0.51×10^{-4}	4.27×10^{-4}	7.35×10^{-4}	1.12×10^{-4}	1.57×10^{-4}
Tensile stiffness (N)	930	7050	11200	1710	1503
Tensile stiffness per density (N·m^3/kg)	4.35	51.84	35.78	7.99	6.74
Compressive stiffness (N)	550	3940	7500	1160	830
Compressive stiffness per density (N·m^3/kg)	2.57	28.97	23.96	5.42	3.74
Torsional stiffness (N·m^2)	4.50×10^{-2}	0.88×10^{-2}	5.94×10^{-2}	3.60×10^{-2}	2.80×10^{-2}
Torsional stiffness per density (N·m^5/kg)	2.10×10^{-4}	0.65×10^{-4}	1.90×10^{-4}	1.68×10^{-4}	1.26×10^{-4}
Overall properties	High torsional stiffness. Low bending stiffness.	High bending, tensile, and compressive stiffness. Low torsional stiffness, low buckling force.	High bending, tensile, compressive, and torsional stiffness.	Relatively high tensile, compressive, and torsional stiffness. Low bending stiffness.	Low bending, tensile, compressive, and torsional stiffness.

3. Application of Lattice Structure to Morphing Wings

As an example of a morphing wing, we developed wing twist morphing using the CUB

E lattice, which exhibits a high equivalent bending stiffness and low equivalent torsional stiffness. When lattice structures are applied to wing structures, the wing structure must be resistant to bending to withstand aerodynamic loads. However, a morphing wing deforms itself; therefore, a wing-twist structure must be stiff in bending but deformable in twist. Based on the experimental results, we investigated the application of the CUBE lattice, whose unit cell exhibits high bending stiffness and easy deformation in the torsional direction, to morphing wings.

3.1 Design of Morphing Wing for Structural Characterization

The lattice structure used for the morphing wing was a CUBE lattice, as described above. We fabricated a prototype for wing twist morphing. The size of the unit cubic cell was 5 mm; the lattice section had a wing span, wing strength length, and wing thickness of 120, 100, and 14 mm, respectively. The morphing wing prototype designed for the evaluation of the structural characteristics is shown in Fig. 10.

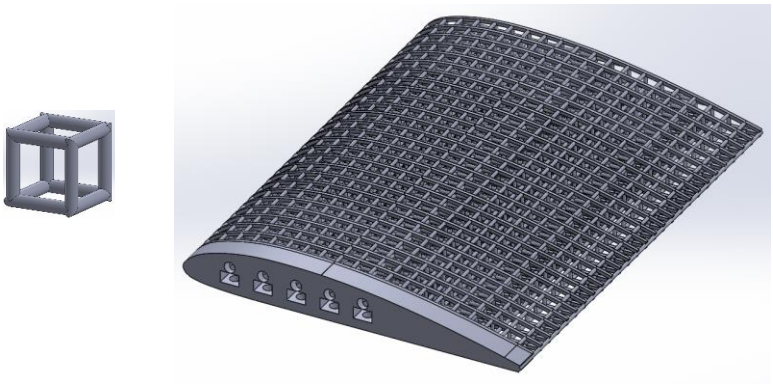

Figure 10 - Morphing wing composed of CUBE lattice

3.2 Bending Test of Morphing Wing

The bending stiffness of the prototype was investigated. A bending test was performed by fixing the root of the wing and pulling the wing tip; the testing machine used was JT Tohsi (Little Senstar). The loads were measured using a load cell (TKA-20A, Tokyo Koki). Owing to the possibility of wing torsion during the bending test, two laser displacement sensors (i.e., Keyence IL-100 and IL-S100) were used to measure the displacement at the leading and trailing edges of the wing, respectively, and the equivalent bending stiffness was determined by the displacement before torsion occurred. An overview of the bending test is shown in Fig. 11 and the experimental results are shown in Fig. 12.

Using the experimental results, the equivalent bending stiffness *EI* can be obtained as follows.

$$EI_{eq} = \frac{PL^3}{3\delta_b}, \qquad [N \cdot m^2] \tag{7}$$

where *P* is the load, *L* is the length of the lattice section of the wing (120 mm), and δ_b is the displacement. The equivalent bending stiffness *EI* was calculated to be 0.1971 N·m^2.

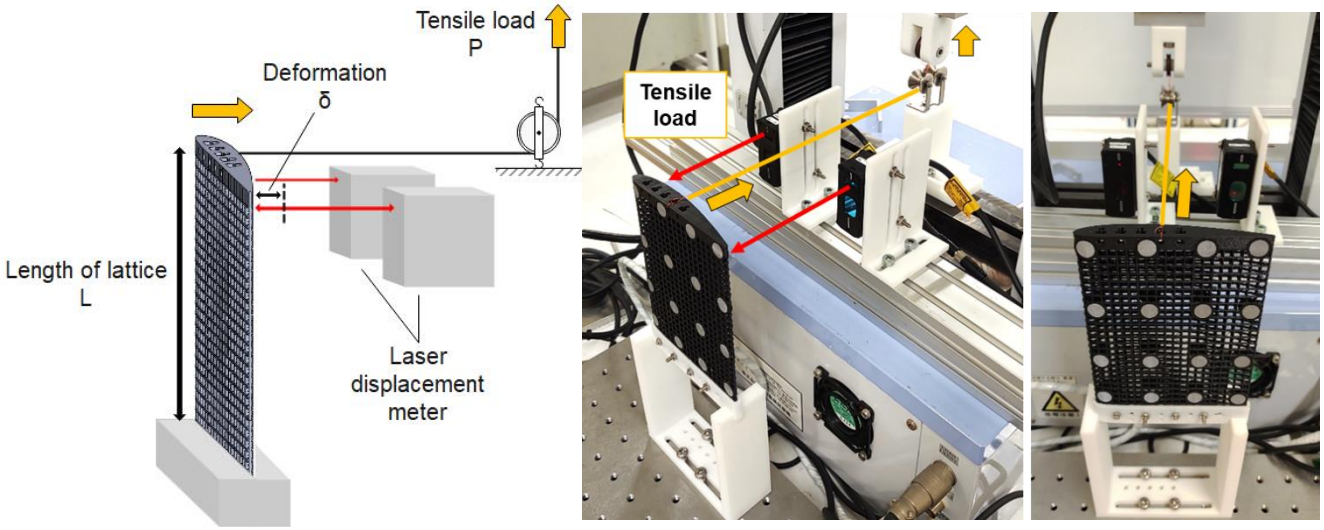

Figure 11 - Overview of morphing wing bending test
(left: schematic representation; right: photograph of test setup)

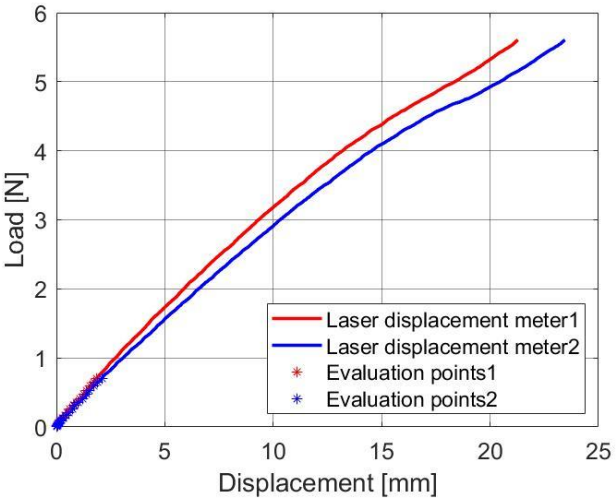

Figure 12 - Load–displacement results from wing bending test

3.3 Torsion Test of Morphing Wing

A torsion test was performed to evaluate the structural characteristics of the morphed wings (Fig. 13); the testing machine used for the torsion tests was JT Tohsi (Little Senstar). The loads were measured using a load cell (TKA-20A, Tokyo Sokki). The displacement was measured three-dimensionally using an AICON/DPA photogrammetric measuring system, and the twist angle of the wing was calculated using the results obtained. In this study, four markers were attached along the wing chord direction for one line, and the torsional angle was defined as the angle between the mean line obtained from the four markers before and after torsion. Markers were attached to four lines: the wing root (Z = 20 mm), two locations at the middle of the wing (Z = 60 and 100 mm), and the wing tip (Z = 140 mm). A total of 16 markers were used to measure the torsional angle.

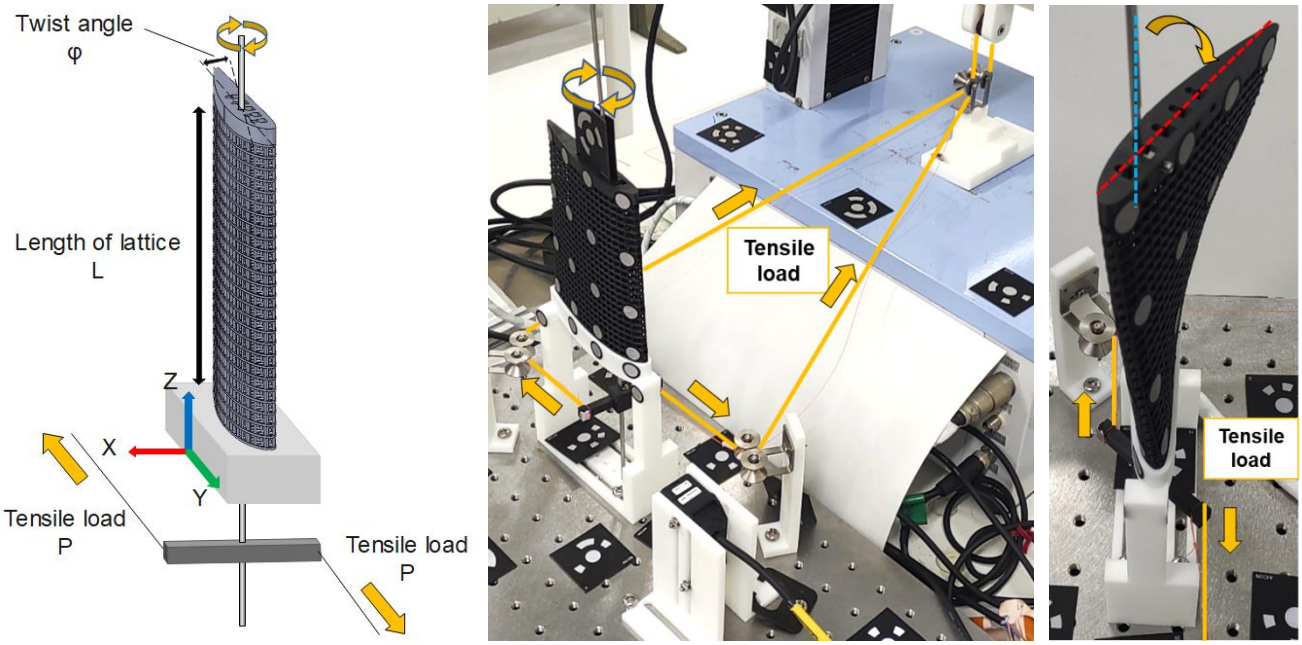

Figure 13 - Overview of morphing wing torsion test
(left: schematic representation; right: photograph of test setup)

3.4 Experimental Results of Morphing Wing

The experimental results are shown in Fig. 14. Figure 14(a) shows the marker positions of the entire wing before and after the torsion test. The blue and red symbols indicate the positions before and

after the torsion test, respectively. Figure 14(b) shows the twist angle distribution along the z-direction. The twist tests were performed thrice.

A plot showing the torque–twist angle relationship is presented in Fig. 15. The twist angles at the wing tip obtained from the three tests are shown in this figure. The dashed line connects the torque–twist angle points before and after the twist test.

Based on these results, the equivalent torsional stiffness GJ_{eq} can be expressed as

$$GJ_{eq} = \frac{M_t}{\varphi} \times L, \qquad [N \cdot m^2] \tag{8}$$

where φ is the specific twist angle, M_t is the applied torsional moment, and L is the length of the wing lattice section. Using the test results, the equivalent torsional stiffness GJ_{eq} of the morphing wing was calculated to be 0.2186 N· m^2.

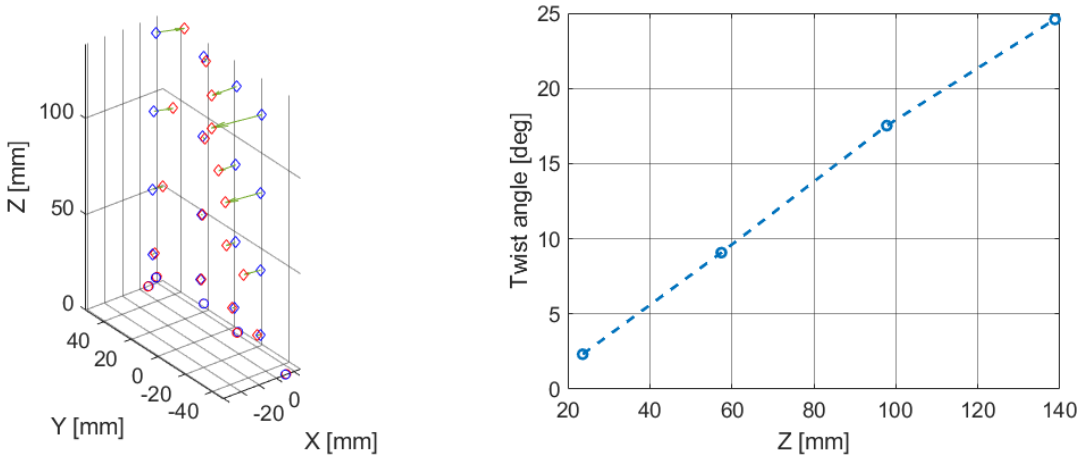

(a) Marker positions before and after torsion test (b) Twist angle distribution

Figure 14 - Deformation of entire wing and twist angle from wing tip to wing root

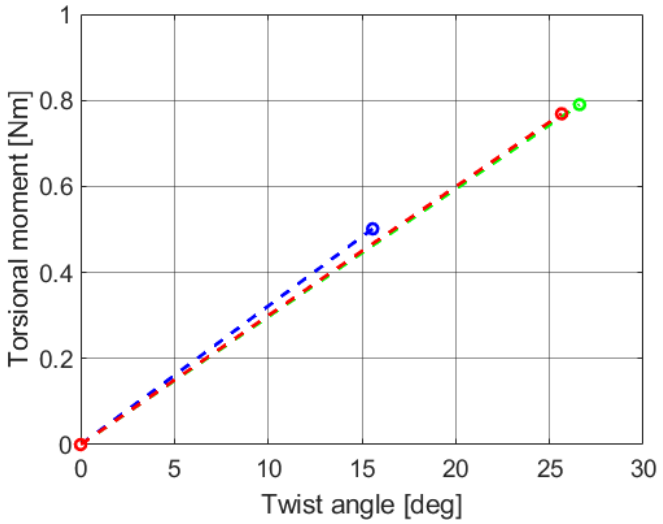

Figure 15 - Torque–twist angle relationship of morphing wing

3.5 Consideration of Morphing Wing

Based on a comparison between the equivalent bending stiffness and equivalent torsional stiffness of the morphing wing created using the CUBE lattice and basic specimen, the ratio between the abovementioned stiffnesses for the basic specimen (CUBE lattice) was 6.6:1, whereas that for the

morphing wing (CUBE lattice) was 0.9:1. This indicates that the torsional stiffness increased in the morphing wing, as compared with in the basic specimen.

When a bending load was applied to the wing, the bending stiffness was affected significantly by the wing thickness but less by the wing chord length. However, the torsional stiffness was affected by the distance from the center of torsion to the outer edge, which is governed primarily by the wing chord length. This resulted in a difference in the relative torsional stiffness between the morphing wing and basic specimen.

The thickness of the specimen was 11 mm, whereas the maximum thickness of morphing wing was 14 mm; therefore, the change in the bending stiffness was limited. By contrast, the width of the specimen was 16 mm and the wing chord length was approximately six times larger than that, i.e., 100 mm; as such, the torsional stiffness increased. These factors may have caused the torsional stiffness of the CUBE lattice to exceed the bending stiffness of the morphing wing, although its unit cell exhibits high bending stiffness and low torsional stiffness.

4. Conclusions

Five basic lattice structures were created and subjected to four-point bending, tensile, compression, and torsion tests. Using the test results, the equivalent stiffness values and stiffness per density values of the specimens were calculated and their structural properties were investigated. The results confirmed that the isotropic and anisotropic properties, in particular the stiffness, varied depending on the basic structure. By selecting the appropriate basic structure based on its structural properties as the lattice structure, the stiffness can be increased or decreased. Meanwhile, by applying the aforementioned structural characteristics with certain anisotropic properties, a lattice structure can be applied to a morphing structure such that arbitrary deformations in response to inputs, such as actuators, can be generated.

As an example of a morphing wing, we developed a prototype of wing twist morphing based on the CUBE lattice, which exhibits high equivalent bending stiffness and low equivalent torsional stiffness; subsequently, we performed bending and torsion tests on the prototype. The ratios of the equivalent bending stiffness to the equivalent torsional stiffness of the basic specimen and morphing wing were 6.6:1 and 0.9:1, respectively, which indicates that the equivalent torsional stiffness is relatively high in the morphing wing. This is attributable to the larger wing chord length specified to fabricate the airfoil, which increased the equivalent torsional stiffness. Nonetheless, the thickness of the wing did not change and the change in the equivalent bending stiffness was suppressed.

5. Contact Author Email Address

For further communication, the author's email address is shown as follows.

Mailto: tanakah@nda.ac.jp

6. Copyright Statement

Acknowledgements

This study was supported by KAKENHI 21H01535.

References

[1] Jia, Z., Liu, F., Jiang, X., and Wang, L., "Engineering Lattice Metamaterials for Extreme Property, Programmability, and Multifunctionality," *Journal of Applied Physics*, Vol. 127, No. 15, 2020.

[2] Moon, S. K., Tan, Y. E., Hwang, J., and Yoon, Y. J., “Application of 3D Printing Technology for Designing Light-Weight Unmanned Aerial Vehicle Wing Structures,” *International Journal of Precision Engineering and Manufacturing - Green Technology*, Vol. 1, No. 3, 2014, pp. 223–228.

[3] Tsushima, N., and Tamayama, M., “Recent Researches on Morphing Aircraft Technologies in Japan and Other Countries,” *Mechanical Engineering Reviews*, Vol. 6, No. 2, 19–00197, 2019.

[4] Aso, A., Tanaka, H., and Mizoguchi, M., " Twistable morphing spar by double cylinder consisting of open and closed section members, *Transactions of the Japan Society of Mechanical Engineers*," Vol. 83, No. 845, 2017 (in Japanese).

[5] Cramer, N. B., Cellucci, D. W., Formoso, O. B., Gregg, C. E., Jenett, B. E., Kim, J. H., Lendraitis, M., Swei, S. S., Trinh, G. T., Trinh, K. V., and Cheung, K. C., “Elastic Shape Morphing of Ultralight Structures by Programmable Assembly, *Smart Materials and Structures*” Vol. 28, No. 5, 2019.

[6] Jenett, B., Calisch, S., Cellucci, D., Cramer, N., Gershenfeld, N., Swei, S., and Cheung, K. C., “Digital Morphing Wing: Active Wing Shaping Concept Using Composite Lattice-Based Cellular Structures,” *Soft Robotics*, Vol. 4, No. 1, 2017, pp. 33–48.